

*75 76 77 78 79 80

Evaluation of the Virtual Crystal Approximation for Predicting Alloy Phonon Properties and Thermal Conductivity

Jason M. Larkin¹ and A. J. H. McGaughey^{1,*}

¹*Department of Mechanical Engineering*

Carnegie Mellon University

Pittsburgh, PA 15213

(Dated: March 6, 2013)

Abstract

The virtual crystal approximation for mass disorder is evaluated by examining two model alloy systems: Lennard-Jones argon and Stillinger-Weber silicon. In both cases the perfect crystal is alloyed with a heavier mass species up to equal concentration and phonon frequencies, lifetimes and group velocities and thermal conductivity are predicted. These two alloy systems have different ranges of phonon frequencies, lifetimes. For Stillinger-Weber silicon, the virtual crystal approximation predicts phonon properties and thermal conductivity in reasonably good agreement with molecular dynamics-based methods. For Lennard-Jones argon, the virtual crystal approximation underpredicts the high-frequency phonon lifetimes, leading to an underpredicting of its thermal conductivity. Resolution of this underprediction is achieved by considering methods that treat the disorder explicitly.

I. INTRODUCTION

Disordered materials (e.g., alloys amorphous solids, aerogels) are used in applications ranging from thermoelectric devices to thermally insulating barriers due to their low thermal conductivities.(cite) Disordered lattices are a subgroup of disordered materials where the atomic positions follow a lattice structure but the constituent species are spatially random. Examples include isotopic solids, where the species have the same electronic structure but small mass variations,¹ and alloys, our focus here, where two distinct species are present. Alloys are also useful for their mechanical properties, which play a role in their thermal transport.(cite) Alloying is an effective method to reduce thermal conductivity while maintaining good electrical transport properties, as is required to improve the efficiency of thermoelectric devices.²⁻⁴

The heat in a dielectric or semiconducting solid is conducted by the vibrational modes of the system. Understanding how these vibrations contribute to thermal transport is crucial for predicting the thermal conductivity of ordered and disordered lattices. Theoretical modeling of thermal transport in disordered lattices dates back to the work of Abeles, who showed that mass and strain disorder dominate the thermal conductivity of SiGe and (Ga,In)As alloys, respectively.⁵ The Abeles theory assumes that the vibrational modes in the alloys are phonons, delocalized propagating modes, and predicts their properties by treating the disorder as a perturbation. Except for low-frequency (long-wavelength) acoustic modes, the general validity of this assumption is unclear.

Predicting the thermal conductivity of a dielectric or semiconducting solid requires the properties of the full spectrum of vibrational modes.⁶⁻⁸ Accurate predictions of these properties for crystalline systems can be made with anharmonic lattice dynamics (ALD) theory using input from Density Functional Theory (DFT) calculations.^{4,9-14} Computational costs limit DFT calculations to be less than 100 atoms, however, making it difficult to explicitly incorporate the effects of disorder.^{4,10,11,15,16}

Disorder is typically included using the Virtual Crystal (VC) approximation, whereby the disordered solid is replaced with a perfect virtual crystal with properties equivalent to an averaging over the disorder (e.g., atomic mass and/or bond strength).⁵ The ALD calculations are performed on a small unit cell with the averaged properties (i.e., all vibrational modes are phonons) and phonon-phonon and phonon-disorder scattering are included as

perturbations.^{1,4,5,10} We will refer to this approach as VC-ALD. Recent work using DFT calculations and the VC-ALD approach predicted phonon mode frequencies, group velocities and lifetimes of alloys with relatively large ($\sim 100 \text{ W/m-K}^{10,11}$) and small ($\sim 1 \text{ W/m-K}^4$) thermal conductivities that compared well with experimental measurements. No comprehensive study has been performed to self-consistently assess the applicability of the VC-ALD approach for a range of disorder.

The objective of this study is to investigate the use of the VC approximation for predicting vibrational mode properties and thermal conductivity of alloys by a detailed comparison of three predictive methods: (i) Molecular Dynamics (MD)-based normal mode decomposition (NMD, Section III C 1), (ii) MD-based Green-Kubo (GK), and (iii) VC-ALD. By using computationally-cheap empirical potentials for argon [Lennard-Jones (LJ)]¹⁷ and silicon [Stillinger-Weber (SW)],¹⁸ we can study the effects of disorder both explicitly and as a perturbation. For both materials, the perfect lattice is disordered with a heavier mass species up to equal concentration ($c = 0.5$), spanning a range of perturbative to large disorder. By spanning this range, the limits of the perturbative models are examined. The computational cost of including disorder explicitly, particularly the large number of time steps required for MD simulation, prohibit the use of typical *ab initio* methods such as plane-wave Density Functional Theory (DFT).^{15,19}

The remainder of the paper is organized as follows. In Section II, theoretical formulation of thermal transport in ordered and disordered solids is introduced. In Section III, the frequencies, group velocities, lifetimes, and diffusivities of the vibrational modes of the disordered lattice are predicted when the disorder is explicitly modeled and when it is treated as a perturbation in the VC approximation. The breakdown of the VC-ALD method is examined in Section III C 2) and a simple correction is provided in Section III D). The vibrational mode properties are then used to predict thermal conductivities in Section IV, allowing for a comparison to the predictions of the Green-Kubo method, where no assumptions about the nature of the thermal transport are required. The mode properties and thermal conductivity of SW silicon alloys are predicted in Section V to provide a comparison for the predictions made for LJ argon alloys in Section IV.

II. THEORETICAL AND MODELING FORMULATION

A. Thermal Conductivity Predictions

To predict the thermal conductivity of a disordered lattice, one begins with the theory for a perfect lattice. For a perfect lattice, all vibrational modes are phonon modes, which by definition are delocalized, propagating plane waves.⁶ Using the single-mode relaxation time approximation⁶ to solve the Boltzmann transport equation²⁰ gives an expression for thermal conductivity in direction \mathbf{n} ,

$$k_{ph,\mathbf{n}} = \sum_{\boldsymbol{\kappa}} \sum_{\nu} c_{ph}(\boldsymbol{\kappa}) v_{g,\mathbf{n}}^2(\boldsymbol{\kappa}_{\nu}) \tau(\boldsymbol{\kappa}_{\nu}). \quad (1)$$

Here, the sum is over the phonon modes in the first Brillouin zone, $\boldsymbol{\kappa}$ is the wavevector and ν labels the polarization branch. The phonon mode has frequency $\omega(\boldsymbol{\kappa}_{\nu})$, volumetric specific heat $c_{ph}(\boldsymbol{\kappa}_{\nu})$, the \mathbf{n} -component of the group velocity vector $v_{g,\mathbf{n}}(\boldsymbol{\kappa}_{\nu})$, and the phonon lifetime $\tau(\boldsymbol{\kappa}_{\nu})$.

The relaxation time approximation has been found to be valid for lower thermal conductivity materials (e.g., Si and SiGe alloys),^{9,11,21} while larger conductivity materials such as GaN and Diamond require a full iterative solution to the BTE for more accurate predictions.^{10,22} For the materials considered here, the lattices and the components of their thermal conductivity tensors are cubically symmetric, so that we will refer to k_{ph} as an isotropic scalar thermal conductivity. This isotropy will hold for disordered lattices in the infinite size limit. Since MD simulations are classical and obey Maxwell-Boltzmann statistics,²³ the volumetric specific heat is k_B/V per mode in the harmonic limit, where V is the system volume. This approximation has been shown to be valid for LJ argon and SW silicon at the temperatures of interest here and is used so that direct comparisons can be made between the MD- and LD-based methods.²⁴

For disordered systems, the vibrational modes are no longer pure plane-waves (i.e., phonon modes), except in the low-frequency (long-wavelength) limit. The Allen-Feldman (AF) theory computes the contribution of diffusive, non-propagating modes (i.e., diffusons) to thermal conductivity,²⁵

$$k_{AF} = \sum_{diffusons} \frac{k_B}{V} D_{AF,i}(\omega_i), \quad (2)$$

where $D_{AF,i}$ is the thermal diffusivity and ω_i is the frequency of the i th disordered vibrational

mode, defined at the wavevector [000]. In the high temperature, classical limit, the diffuson volumetric specific heat is k_B/V .

Assuming that all vibrations scatter over a distance of the lattice spacing, the high-scatter (HS) limit of thermal conductivity is

$$k_{HS} = \frac{k_B}{V_b} b v_s a, \quad (3)$$

where V_b is the volume of the unit cell, v_s is the branch-averaged sound speed, b is the number of and a is the lattice constant.²⁶

B. Virtual Crystal Approximation

Under the VC approximation, the disordered solid is replaced with a perfect virtual crystal with properties equivalent to an averaging over the disorder (e.g., atomic mass and/or bond strength).⁵ The VC approximation is visualized in Fig. 1, where the explicitly mass disordered supercell is replaced by a perfect crystal of equivalent “virtual” mass. Abeles first introduced the concept of a VC to predict the thermal conductivity of SiGe, (Ga,In)As and In(As,P) alloys, using Klemens-Callaway theory to model the phonon-phonon and phonon-defect scattering.^{27–29} The Abeles theory is conceptually simple, treating both disorder and anharmonicity as perturbations and expressing the thermal conductivity as a closed-form analytical function of the bulk material properties.⁵ With the use of phenomenological fitting parameters, good agreement between the predictions and experimental measurements was found for SiGe and (Ga,In)As. Deviations from the Abeles theory were observed for In(As,P) alloys at large concentrations of InP, which were attributed to the high mass ratio of 3.7 between In and P.⁵

While the Abeles theory was developed using Klemens-Callaway theory and the VC approximation, which is valid for low-frequency modes and small disorder (see Section), its application leads to good agreement with some experimental and computational results for systems with a range of disorder. Cahill and co-workers found that the thermal conductivity reduction in dilute Ge-doped Si epitaxial layers can be explained by mass perturbative disorder alone.^{30,31} The effect of bond and mass disorder was investigated computationally using Molecular Dynamics (MD) simulation by Skye and Schelling for SiGe,³² who also found that mass disorder is the dominant scattering mechanism. It is important to note that the

overall disorder strength is determined by both the mass ratio, the stiffness ratio, and the alloy concentration (see Section III C 2). For example, as little as $6.2 \times 10^{19} \text{ cm}^{-3}$ Ge is enough to reduce the thermal conductivity of Si (mass ratio of 2.6) by a factor of two.³⁰ In the case of $\text{Ni}_{0.55}\text{Pd}_{0.45}$, with large mass ratio (1.8) and concentration of each species, good agreement between experimental measurements and perturbation theory predictions for vibrational frequencies and linewidths was observed.^{33,34} In the low-frequency limit, the perturbative mass disorder theory³³ reduces to the expression derived by Klemens^{27,28} and used by the Abeles theory.⁵ Given these results, it is unclear what limitations exist using the VC approach with perturbative disorder theory.^{1,5,33}

Unlike the phenomenological Abeles theory, the VC-ALD approach predicts thermal conductivity by summing over the whole phonon spectrum, with phonon-phonon and phonon-defect scattering treated as perturbations (see Section).^{4,10,11} Using DFT methods to predict the mode-specific phonon properties of the VC, Lindsay and Broido found good agreement between VC-ALD and experiment for isotopically defected GaN, which has relatively small concentrations (much less than one percent).¹⁰ Garg used DFT calculations with VC-ALD to predict the thermal conductivity of SiGe alloys for all concentrations, obtaining good agreement with experiment.¹¹ Isotopically-defected GaN and SiGe alloys have relatively large thermal conductivities at 300 K (100 W/m-K). In particular, the thermal conductivity of SiGe alloys is significantly larger than the high scatter limit (Eq.).²⁶ In our survey of experimental mesurement and numerical modeling, VC predictions tend to be accurate when the thermal conductivity is significantly above the high-scatter limit (Eq. (3)).^{5,10,11,26,30,31,34}

A VC-ALD study using phonon properties from DFT calculations for the low thermal conductivity PbTe¹² and PbTe/PbSe alloys⁴ predicted thermal conductivities for the perfect systems in fair agreement with experiment. Experimental results lack for the alloys, making it difficult to asses the validity of the VC-ALD approach.^{35,36} The thermal conductivity of PbTe/PbSe and their alloys have thermal conductivites at thermoelectric operating temperatures which approach the high scatter limit.^{2,4,35,36}

In this study, we will consider a low thermal conductivity alloy using the LJ potential and high thermal conductivity alloy using the SW potential. While the computational studies discussed above were limited to VC-ALD because of DFT calcualtion costs, the use of computationally cheap empirical potentials will allow us to include the disorder explicitly and as a perturbation and to compare the predictions.

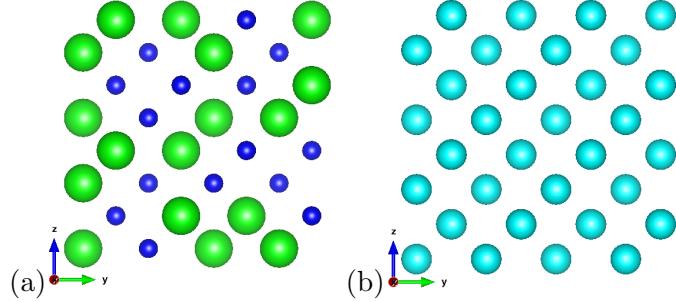


FIG. 1: (a) view of an explicitly disordered supercell of Si and “heavy” Si ([100] direction into the paper).³⁷ (b) view of the equivalent VC supercell with an average mass of the explicitly disordered Si and “heavy” Si supercell (b). Sphere size represents increasing mass only, no bond disorder is considered. In this work, calculations for LJ Ar and SW Si which use the VC approximation are based off of the conventional cubic unit cells (Section II C)

C. Calculation and Simulation Details

The key to explicitly incorporating the effects of disorder is to use large disordered supercells. The methods used in this work scale differently with the size of the supercell. The calculations in this work are trivially parallelizable except the MD simulations³⁸ and the eigenvalue solution of the dynamical matrix.³⁹ Efficient MD codes scale linearly with the number of atoms in the system, N_a . The Gamma-NMD and AF theory require the solution of a large Dynamical matrix of size $(3N_a)^2$, which limits the system sizes considered.

Perfect and disordered lattice supercells are generated using the conventional unit cells for LJ argon ($n = 4$) and SW silicon ($n = 8$), where n is the number of atoms in the unit cell. Supercells are built cubically with size N_0 , where N_0 refers to the number of unit cell repetitions in all three spatial directions. Supercells up to $N_0 = 12$ (6096 atoms) are used for the LJ argon calculations. For SW silicon, $N_0 = 8$ (4096 atoms) is used for the MD-based NMD calculations, and $N_0 \leq 42$ (≤ 592704 atoms) is used for the MD-based GK and VC-ALD. The MD simulations were performed using LAMMPS.³⁸

Disorder is created by randomly specifying the masses of the atoms on the lattice. The composition of the lattices is labeled by $m_{1-c}^i m_c^j$, where (i) $m^i = 1$ and $m^j = 3$ in LJ units for argon and (ii) $m^i = m_{Si}$ and $m^j = 2.6m_{Si}$ for SW silicon and “heavy silicon”, which has the mass of germanium. Concentrations, c , of $c = 0.0, 0.05, 0.15$ and 0.5 are used. Even though only mass disorder is considered in this study, the concentrations considered are much larger than in typical isotopic solids.^{1,10}

For SW silicon, the lattice constant, a , is 5.43\AA for all calculations, which brings the GK thermal conductivity predictions at a temperature of 300K ^{40,41} into better agreement with VC-ALD predictions.⁴² For LJ argon, the lattice constant at a temperature of 10 K is 5.290\AA .⁴³ An amorphous LJ phase, discussed in Section III D, was created by liquifying the crystal and instantly quenching by removing all kinetic energy. The energy of the resulting structure was minimized and then annealed in an NPT (constant number of atoms N , pressure P , and temperature T) ensemble at zero pressure and a temperature of $T = 10\text{ K}$. The effective zero-pressure lattice constant of the amorphous phase at this temperature, based on the atomic density, is 5.389\AA .⁴³

All MD simulations are first equilibrated in a NVT (constant number of atoms N , volume V , and temperature T) ensemble for 10^6 time steps. Data is then collected from simulations

in the NVE (constant number of atoms N, volume V and energy E) ensemble. For LJ argon, a potential energy cutoff of 3.4\AA is used (the force is not adjusted). MD simulation time steps of 4.285 and 0.5 fs were used for LJ argon and SW silicon. It is important to note that the same atomic trajectories are used for the NMD and GK methods.

III. VIBRATIONAL MODE PROPERTIES IN ALLOYS

A. VC and Gamma DOS

In this section, we begin to examine the effects of explicitly including disorder in the LJ system by computing the frequencies and density of states [DOS, $D(\omega)$] for vibrational modes of disordered lattice supercells and their equivalent VCs. The frequencies are computed using harmonic lattice dynamics calculations with GULP.³⁹ For the VC, the allowed wavevectors are set by N_0 and there are 12 polarization branches per wave vector.²⁴ For the disordered supercells, the only allowed wavevector is the gamma-point (i.e., $\kappa = 0$) where there are $12N_0^3$ polarization branches.

The DOS for the VC and the explicitly disordered supercells (referred to herein as Gamma) are shown in Fig. 2 for concentrations of 0.05, 0.15 and 0.5 for $N_0 = 12$ (i.e., 6912 atoms). The VC and Gamma DOS agree at low frequencies, where the Debye approximation predicts $\text{DOS} \propto \omega^2$.¹¹ Similar agreement at low frequencies was found in DFT predictions for $\text{Si}_c\text{Ge}_{1-c}$,¹¹ while Bouchard showed similar continuous behavior as a function of concentration at low frequency for amorphous $\text{Si}_c\text{Ge}_{1-c}$.⁴⁴ The Debye approximation underpredicts the DOS at moderate frequency, which is due to non-linearities in the dispersion.¹⁷

The increasing average atomic mass with increasing concentration for the VC shifts all frequencies downward by a factor $1/[(1 - c)m^i + cm^j]^{1/2}$. The increasing average atomic mass for the Gamma modes also reduces the frequencies, but not in a systematic manner. The effect of the disorder is seen at high frequencies greater than 10 by a broadening and a shift of the Gamma DOS to higher frequencies because of the explicit use of light atoms in the supercell. Duda et al observed similar high-frequency broadening effects in model LJ alloys from MD simulation.⁴⁵ Based on the DOS, the vibrational modes of the explicitly disordered supercells at low frequencies are phonon-like, while the broadening of the DOS

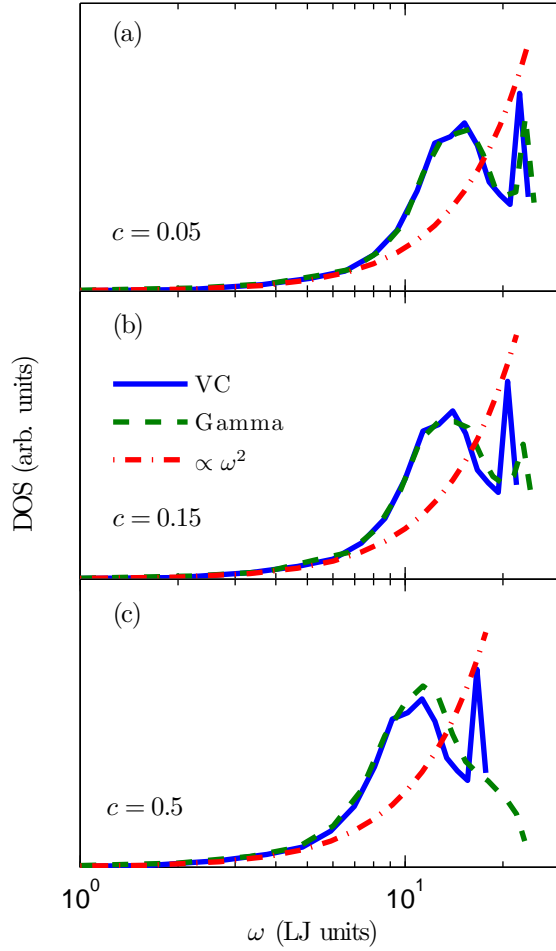


FIG. 2: Density of states (DOS) for modes calculated using the LJ FCC VC versus an explicitly mass disordered LJ FCC supercell (labeled Gamma) with varying mass concentration c . VC and Gamma show similar low frequency behavior for all c . For increasing c , the frequencies of both VC and Gamma decrease, while the high frequency DOS for Gamma spreads and reaches up to a higher maximum frequency because of the explicit disorder. The size of these supercells is $N_0 = 12$ (see Section II C).

at high-frequency indicates that the Gamma vibrational modes may differ from the high-frequency VC phonon modes. This behavior is further explained in the next three sections.

B. Dispersion and Group Velocity

The group velocity vector in a VC is defined as the gradient of the dispersion curve,

$$v_{g,\mathbf{n}}(\boldsymbol{\kappa}) = \frac{\partial\omega(\boldsymbol{\kappa})}{\partial\boldsymbol{\kappa}}. \quad (4)$$

We calculate the group velocities for the VC using finite differences on frequencies calculated from harmonic lattice dynamics.⁴⁶

For ordered and disordered solids, the three acoustic group velocities (two transverse and one longitudinal) can be predicted using the elastic constants³⁹ or by finite differencing of the first three branches of a disordered supercell.^{47,48} Except for the three acoustic branches, there is not an accepted method to predict the effective group velocity of a vibrational mode in a disordered system, although there have been attempts.^{26,45,47–49} In the Cahill-Pohl (CP) model, for example, the group velocity of all disordered modes is the sound speed, v_s , which is also assumed for the high-scatter model (Eq. (3)).²⁶ However, this is a good assumption for any material, even in the amorphous phase.^{45,47–50}

Calculating the structure factor of the supercell Gamma modes is a method to test for the plane-wave character of disordered modes at a particular wavevector and polarization corresponding to the VC.^{8,50} Feldman et al. used the structure factor to predict an effective dispersion for a model of a-Si, but did not predict group velocities.⁵⁰ Volz and Chen used the dynamic structure factor to predict the dispersion of crystalline SW Si using MD simulation.⁵¹

The structure factor is defined as⁸

$$S^{L,T}(\boldsymbol{\kappa}_{VC}) = \sum_{\nu} E^{L,T}(\boldsymbol{\kappa}_{VC}) \delta(\omega - \omega(\boldsymbol{\kappa}_{\nu}=\mathbf{0})), \quad (5)$$

where E^T refers to the transverse polarization and is defined as

$$E^L(\boldsymbol{\kappa}_{VC}) = \left| \sum_b \hat{\mathbf{k}}_{VC} \cdot e^{(\boldsymbol{\kappa}_{\nu}=\mathbf{0})_b} \exp[i\boldsymbol{\kappa}_{VC} \cdot \mathbf{r}_0(l=0)] \right|^2 \quad (6)$$

and E^L refers to the longitudinal polarization and is defined as

$$E^T(\boldsymbol{\kappa}_{VC}) = \left| \sum_b \hat{\mathbf{k}}_{VC} \times e^{(\boldsymbol{\kappa}_{\nu}=\mathbf{0})_b} \exp[i\boldsymbol{\kappa}_{VC} \cdot \mathbf{r}_0(l=0)] \right|^2. \quad (7)$$

Here, $\mathbf{r}_0(l=0)$ refers to the atomic positions of the mass disordered atoms in the supercell which are still spatially ordered, $\boldsymbol{\kappa}_{VC}$ are the VC allowed wavevectors, and $\hat{\mathbf{k}}_{VC}$ is the

unit wavevector. Explicit disorder is accounted for in the mode frequencies $\omega(\kappa=0)$ and eigenvectors $e(\kappa=0 \alpha)$, which are calculated with $\kappa = \mathbf{0}$. The disordered mode eigenvector $e(\kappa=0 \alpha)$ has length $3N_a$ and describes the spatial variation of the vibrational pattern.

Physically, $S^{L,T}(\kappa)$ represents the frequency spectrum required to create a wavepacket with a well-defined wavevector and polarization.^{8,50,52} For a perfect lattice, the structure factor peaks are delta functions centered at the phonon mode frequencies, indicating that they are pure plane-waves. A sampling of the structure factors for the LJ argon alloys are plotted in Fig. 3 for wavevectors along the [100] and [111] directions in the $N_0 = 10$ systems. With increasing disorder, the structure factor spreads in width, particularly at high frequencies where the modes are no longer pure plane-waves.

From Fig. 3, an effective dispersion curve can be extracted by locating the peaks in the structure factors at neighboring VC wavevectors, which are plotted in the middle panels. The effects of polarization, average atomic mass, and anisotropy can be observed. As the average atomic mass becomes larger, the peaks in the structure factor shift to lower frequencies. The peaks in the structure factor are larger than the VC predicted frequencies by at most 5%. Similar agreement is found with the disordered SW silicon lattice supercells (not shown), where the structure factors are more complicated because of the optical modes. Well-defined peaks at all wavevectors are due to the lattice structure of the disordered systems. Typically, the structure factor for amorphous materials has well-defined peaks only for small wavevector.^{8,50}

Because of the good agreement between the VC-predicted dispersion curves and the peaks in the structure factors from Fig. 3, we will use the group velocities predicted by the VC dispersion for both LJ argon and SW silicon with the VC-NMD and VC-ALD calculations for consistency and simplicity. We will examine the validity of this group velocity choice in Section III D.

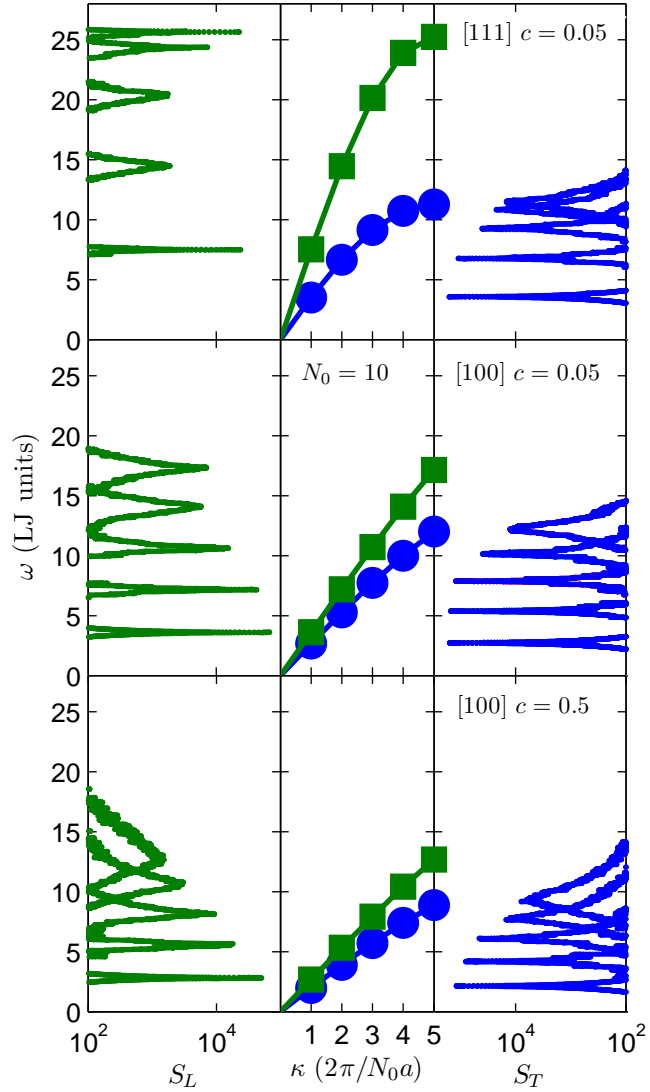


FIG. 3: Left and Right Panels: The structure factor for longitudinal (S_L) and transverse (S_T) polarizations along high symmetry directions ([100], [110] where $\kappa = \pi/a[100]$ and a is the lattice constant) of the mass disordered LJ argon supercells ($N_0 = 10, c = 0.05, 0.5$). For increasing mass disorder c , there is a decrease in the center of the peaks and an increase in the peak linewidths. Center Panel: The VC predicted dispersion at the same wavectors used to calculate $S_{L,T}$.

C. Lifetimes

1. From VC-NMD and Gamma-NMD

Once the group velocities are predicted using the VC dispersion, the phonon mode lifetimes are required to predict the thermal conductivity using Eq. (1). As an alternative to the VC-ALD approach for predicting phonon lifetimes, which are discussed in the next section, we first use the MD simulation-based normal mode decomposition (NMD) method.^{53,54} The effects of disorder are contained in the atomic trajectories (positions and velocities) of the MD simulation performed on the explicitly disordered supercells (see Section). In NMD, the atomic trajectories are first mapped onto the vibrational normal mode coordinate and its time derivative,⁵⁵

$$q(\kappa; t) = \sum_{\alpha, b, l}^{3, n, N} \sqrt{\frac{m_b}{N}} u_\alpha(b; t) e^*(\kappa \cdot \alpha) \exp[i\kappa \cdot \mathbf{r}_0(l)] \quad (8)$$

and

$$\dot{q}(\kappa; t) = \sum_{\alpha, b, l}^{3, n, N} \sqrt{\frac{m_b}{N}} \dot{u}_\alpha(b; t) e^*(\kappa \cdot \alpha) \exp[i\kappa \cdot \mathbf{r}_0(l)], \quad (9)$$

where $\mathbf{r}_0(l)$ are the equilibrium positions of the atoms in the l th unit cell of the lattice supercell. The total energy of a given vibrational mode is calculated from

$$E(\kappa; t) = \frac{\omega(\kappa)^2}{2} q(\kappa; t)^* q(\kappa; t) + \frac{1}{2} \dot{q}(\kappa; t)^* \dot{q}(\kappa; t) \quad (10)$$

The normal mode lifetime is predicted using

$$\tau(\kappa) = \int_0^{t*} \frac{\langle E(\kappa; t) E(\kappa; 0) \rangle}{\langle E(\kappa; 0) E(\kappa; 0) \rangle} dt, \quad (11)$$

where the upper integration limit $t*$ is much larger than the phonon lifetime.²⁴ Equation (11) is derived assuming that the energy correlation follows an exponential decay.⁵⁴

We perform NMD using the frequencies and eigenvectors from both the VC unit cell ($\omega(\kappa)$, $e(\kappa \cdot \alpha)$) and the Gamma supercell ($\omega(\kappa=0)$, $e(\kappa=0 \cdot \alpha)$). The trajectories from these MD simulations are also used in the GK method calculations (Section IV). The MD simulations were 10 times longer than the longest phonon lifetime in the system, which can be estimated *a priori* from the VC-ALD predicted phonon lifetimes. For LJ argon and SW silicon, data

was collected for 2^{20} and 2^{22} time steps and the atomic trajectories were sampled every 2^8 and 2^4 time steps, respectively. Ensemble averaging was performed using ten independent initial randomized velocity distributions.

For the normal modes of the lattice supercell, Eq. (11) is exact, but becomes an approximation when using the non-exact VC normal modes to perform the mappings in Eqs (8) and (9). Even for larger disorder ($c = 0.5$) where the energy autocorrelations are more complicated but generally follow exponential decay, an effective lifetime can still be predicted using Eq. (11) (see Appendix A). The lifetimes predicted using VC-NMD and Gamma-NMD are shown in Fig. 4 for the LJ argon crystal and alloys at a temperature of 10 K. The range of frequencies for VC-NMD and Gamma-NMD differ slightly due to differences in the DOS (see Fig. 2). For a small interval of frequency, there is a wider range of predicted lifetimes for Gamma-NMD. This spread is because there is no symmetry averaging of the mode properties, which is possible for the VC by considering the crystal lattice's irreducible Brillouin zone (BZ) which define a set of irreducible wavevectors that are used to average the mode properties of the reducible wavevectors.¹⁷

The lifetimes predicted by both VC-NMD and Gamma-NMD show ω^{-2} scaling at low frequency and ω^{-4} scalings (for the alloys) and even faster for mid-range frequencies. The majority of the lifetimes predicted by both VC-NMD and Gamma-NMD are larger than the Ioffe-Regel (IR) limit,⁵⁶

$$\tau = \frac{2\pi}{\omega}. \quad (12)$$

The physical interpretation of the IR limit is that of a mode which scatters in a time equal to its oscillation period. Our results suggest that the IR limit is a good lower-limit for the lifetimes predicted by VC-NMD and Gamma-NMD for LJ argon (Fig. 4) and VC-NMD for SW silicon (see Fig. 8(a) in Section V). A constant lifetime is observed at the highest frequencies, for both VC-NMD and Gamma-NMD, except at $c = 0.5$ for VC-NMD. We are not aware of any theoretical prediction of this high-frequency behavior.

Overall, good agreement is seen in the predicted lifetimes from VC-NMD and Gamma-NMD both in magnitude and trends. The use of the VC normal modes is an approximation that becomes worse as the concentration is increased (see Appendix A), but our results suggest that the effect is only pronounced at the highest frequencies. The only approximation associated with Gamma-NMD is the use of the harmonic lattice dynamics predicted frequencies and eigenvectors to map the atomic trajectories from the fully anharmonic MD

simulations, which has been shown to be valid below temperatures of 40 K for LJ argon.⁵⁴ Based on the good agreement with Gamma-NMD, the lifetimes predicted by VC-NMD are used along with the VC predicted group velocities to predict thermal conductivity in Section IV. For Gamma-NMD, there is no general way to predict the mode group velocities so that the thermal conductivity can be predicted using Eq. 1.

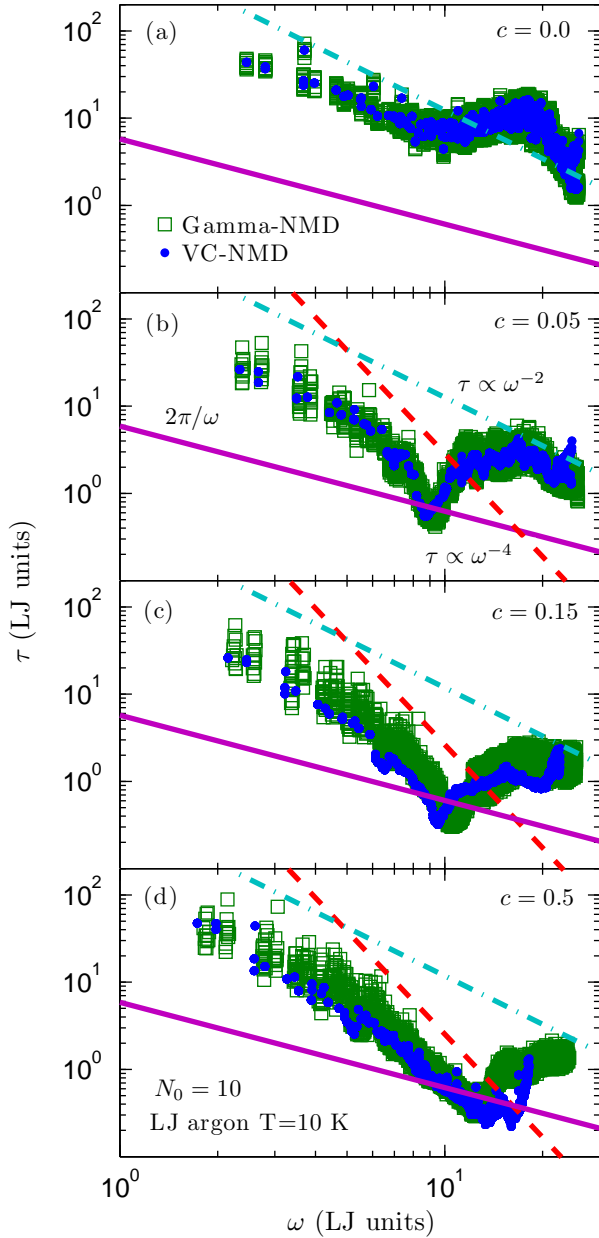


FIG. 4: Lifetimes predicted using VC-NMD and Gamma NMD from MD simulations of mass disordered lattice supercells (Section III C 1). Both ω^{-2} and ω^{-4} scalings can be observed at low frequencies, which are predicted by the perturbative models used for VC-ALD (Section III C 2). For both VC-NMD and Gamma NMD, most mode lifetimes are greater than the Ioffe-Regel limit $\tau = 2\pi/\omega$.⁵⁶ While there is more “noise” in the Gamma-NMD data (Section III C 1), the lifetime magnitudes and trends agree well, an important consideration when comparing VC-NMD and VC-ALD in Fig. 5 .

2. From VC-ALD

Under the VC approximation, the ALD calculations⁵⁴ are based on the (small) conventional unit cells of LJ argon and SW silicon (see Section) unit cell with the average atomic mass of varying concentration c . Disorder is not included explicitly but is treated using perturbation theory.^{1,33} Assuming phonon-phonon and phonon-defect scattering mechanisms to operate independently, the effective phonon lifetime can be found using the Matthiessen rule⁶,

$$\frac{1}{\tau(\nu)} = \frac{1}{\tau_{p-p}(\nu)} + \frac{1}{\tau_{p-d}(\nu)}, \quad (13)$$

where $\tau_{p-p}(\nu)$ accounts for intrinsic phonon-phonon scattering and $\tau_{p-d}(\nu)$ accounts for phonon-defect scattering.

Phonon-phonon scattering can be modeled using anharmonic perturbation theory (i.e., ALD) including only three-phonon processes.^{4,11,54} It has been demonstrated that the effects of higher-order phonon processes become important at high temperatures.^{54,57} The present study is concerned with temperatures much less than the melting temperature of either LJ argon⁴³ or SW silicon.¹⁸ We predict the phonon-phonon lifetimes using the method described in Ref. 54, with all classical expressions to remain consistent with the classical MD-based methods.

Using harmonic perturbation theory, Tamura derived a general expression for mass point defect scattering.¹ By considering the symmetry properties of the FCC lattices considered in this work, his expression reduces to

$$\frac{1}{\tau_{p-d}(\nu)} = \frac{\pi}{2} g_2 \omega^2(\nu) D(\omega), \quad (14)$$

where

$$g_n = \sum_{\mu} c^{\mu} (1 - m^{\mu}/\bar{m}^{\mu})^n. \quad (15)$$

Here, c^{μ} and m^{μ} are the concentration and mass of the μ -th species and \bar{m}^{μ} is the average mass. Bond disorder can be accounted for using a similar expression with an average atomic radius or suitable scattering cross-section.^{27,28} For the binary LJ argon and SW silicon alloys considered here, there is one atom type in the unit cell with $\mu = i, j$, so that the alloying atom labeled by m_{1-c}^i can be considered to be an “isotope” of the atom labeled m_c^j . This convention is adopted from the perturbation theory¹ that was used to predict effect of defect

scattering in isotopic Ge, while we consider large ratios and concentrations of mass defects in the present study. The disordered lifetimes are calcualted using Eqs (14) and (15).

The lifetimes predicted by VC-ALD for LJ argon at a concentration of 0.05 are plotted in Fig. 5(a). Also plotted are the lifetimes for the perfect system and from the VC-NMD predictions at this concentration. At low frequencies, where the density of states is Debye-like [$D(\omega) \propto \omega^2$, Fig. 2], $\tau_{p-p}(\kappa)$ scales as ω^{-2} , which is due to intrinsic three-phonon scattering processes.⁵⁸ The scaling is also observed in the VC-NMD and Gamma-NMD. Under the Debye-approximation the phonon scattering due to mass point-defects is predicted to scale as ω^{-4} and is observed in the VC-NMD, Gamma-NMD and VC-ALD predicted lifetimes in the mid-frequency range. VC-ALD does not predict the frequency-independent lifetimes at high frequency for LJ argon observed in VC-NMD and Gamma-NMD.

The thermal conductivity frequency spectrum is plotted in Fig. 5 (c), and demonstrates that the conductivities of LJ argon and its alloys are dominated by high frequency modes. From this plot, it can be seen that VC-ALD underpredicts the thermal conductivity at high-frequencies, consistent with lifetime underprediction by VC-ALD compared to VC-NMD.

The Tamura theory was developed to predict the reduction of lifetimes in isotopic Ge, which is only perturbatively disordered ($\frac{\Delta m}{\bar{m}} \approx 0.05$). The importance of higher-order (i.e., $n > 2$) interactions in the Tamura theory become important with increasing disorder strength.¹ For isotopically-disordered Ge, the higher-order contributions were estimated to be negligible at all frequencies.¹ For LJ argon and the large concentrations and mass ratios considered in this work, the terms higher order terms are order unity and larger at high frequencies. For example, for a concentration of 0.15, $g_2 = 0.3018$, $g_3 = -0.3250$ and $g_4 = 0.4411$. It is possible that the higher-order interactions in the Tamura theory are responsible for the discrepancy of the lifetimes predicted by VC-NMD and Gamma-NMD versus VC-ALD at high frequency.

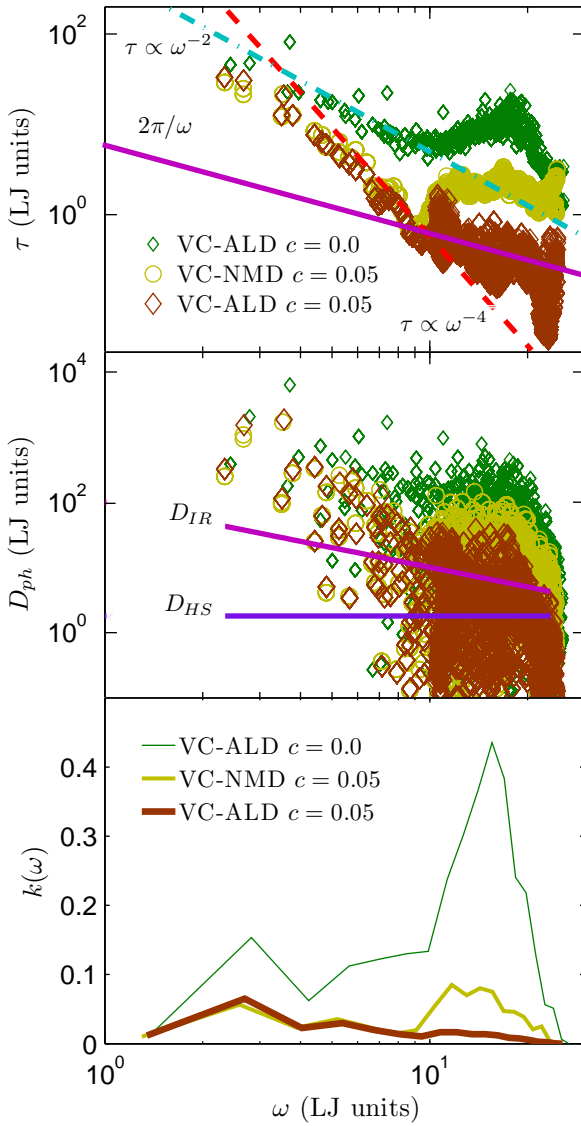


FIG. 5: (a) predicted lifetimes for VC modes using VC-NMD and VC-ALD for LJ argon ($T = 10$ K, $N_0 = 10$ and $c = 0.05$). The lifetimes predicted by VC-ALD and VC-NMD (not shown) agree at $c = 0.0$. (b) predicted VC mode thermal diffusivities, compared to the AF,HS limit. (c) the thermal conductivity frequency spectrum, which is peaked at high frequency, in contrast to SW silicon (Fig 8).

D. Diffusivities

While studies have been performed on alloying the amorphous phase, the AF theory has not been applied to disordered lattices.⁷

In the current study of disordered lattices, the AF theory predictions provide a lower limit for the contribution of a given vibrational mode within the computational framework of the VC approximation. This is essential given the computational cost of the AF theory (Section).

Once the group velocities and lifetimes are predicted, they can be used to predict the mode thermal diffusivity. Even for large disorder, modes at low frequency have well-defined group velocities and lifetimes, which is demonstrated by the Gamma-mode structure factor peaks (see Fig.) and lifetimes predicted by VC-NMD, Gamma-NMD, and VC-ALD. At high frequencies it is not possible to specify a mode group velocity and lifetime independently,^{50,59} and the mode thermal diffusivity must be considered to predict thermal conductivity.

In the classical harmonic limit, where the specific heat is mode-independent, a vibrational mode's contribution to thermal conductivity is determined by its thermal diffusivity,

$$D_{ph,\mathbf{n}}(\nu) = v_{g,\mathbf{n}}^2(\nu) \tau(\nu), \quad (16)$$

such that

$$k_{ph,\mathbf{n}} = \sum_{\kappa} \sum_{\nu} \frac{k_B}{V} D_{ph,\mathbf{n}}(\nu), \quad (17)$$

analogous to Eq. (1). For the VC-NMD and VC-ALD calculations, $v_{g,\mathbf{n}}(\nu)$ is calculated from the VC dispersion (Section III B) so that any differences in thermal diffusivity will come from the predicted lifetimes. The lower limit for phonon thermal diffusivity is zero since the group velocities can be zero (e.g., optical modes at the Brioullin zone center).¹⁷

In a disordered system, modes can transport heat by harmonic coupling due to disorder in the Allen-Feldman (AF) theory of diffusons [Eq. (2)].²⁵ In the high-scatter (HS) limit,²⁶ the diffusivity of each mode is

$$D_{HS} = \frac{1}{3} v_s a, \quad (18)$$

which leads Eq. (3). The physical interpretation of Eq. (18) is that all vibrational modes transport heat at the sound speed and scatter with a mean free path of the lattice spacing. As seen in Fig. 5(b) for the LJ argon alloy at a concentration of 0.05, VC-NMD and VC-ALD predict [from Eq. (16)] a significant number of modes with $D_{ph}(\nu) < D_{HS}$.

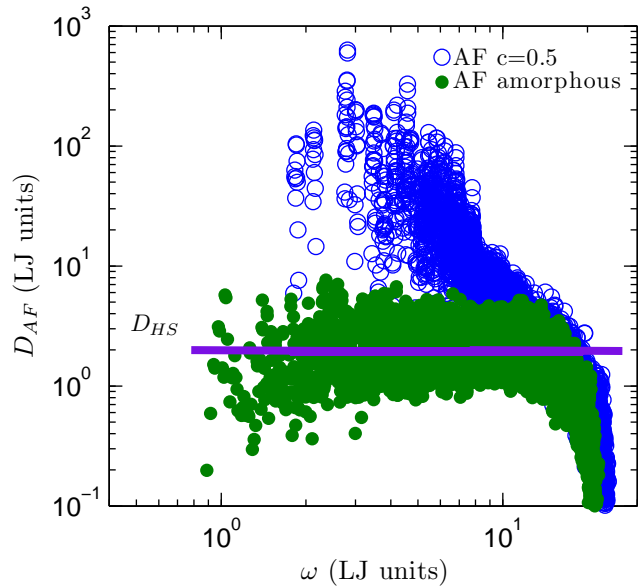


FIG. 6: AF theory predictions of disorded mode thermal diffusivities for LJ argon disorded lattice supercell and amorphous phase. The mode thermal diffusivities predicted for the disorded lattice supercell are all finite, except at the highest frequency where they tend to 0 as in the amorphous phase.

While the HS model assumes a mode-independent thermal diffusivity, the AF theory is capable of predicting mode-specific thermal diffusivities.^{7,50,60} Since the AF theory is harmonic, mode thermal diffusivities typically diverge as the frequency approaches zero because these vibrations are long-wavelength plane waves that are weakly scattered by the disorder.^{61,62} The mode-specific thermal diffusivities of an LJ argon amorphous phase (see Section) are plotted in Fig. 6. Except at the highest frequencies, the thermal diffusivity of all modes can be approximated using a mode-independent diffusivity of D_{HS} . Also plotted in Fig. 6 are the AF predicted thermal diffusivities for the explicitly disordered LJ argon lattice supercell alloy at a concentration of 0.5. As expected, the AF theory predictions diverge at low frequency. The thermal diffusivity of all modes are larger than D_{HS} except at the highest frequencies, where they tend to zero as in the amorphous phase. This result supports the plausible lower-bound of the VC predicted phonon thermal diffusivity to be D_{HS} .

E. Discussion

For disordered systems, it is generally only possible to assign a unique lifetime and group velocity to vibrational modes in the low-frequency, propagating limit.^{50,59} The VC predicted group velocities, particularly for $v_g(\nu) \ll v_s$ or $v_g(\nu) \approx 0$, are an underprediction of the representative velocity scale for the thermal diffusivity of high-frequency modes in the disordered lattice as calculated from Eq. . This is demonstrated by considering the AF theory predicted mode thermal diffusivities, which are finite for the heavily disordered LJ alloy at a concentration of 0.5 (Fig.). For phonons, the thermal diffusivity can be zero because of the VC predicted group velocities, which is not consistent with the AF theory predictions.

Predictions from model disordered systems demonstrate the existence of a plateau of the thermal diffusivity at high frequency, which is consistent with the minimum phonon mean-free path hypothesis⁶³ used in most models of thermal transport in disordered materials.^{26,64,65} The concept of a vibrational mean free path is only valid, however, for low-frequency propagating modes in disordered systems.⁵⁰ The more fundamental property is the vibrational mode lifetime⁵⁶ or thermal diffusivity.^{7,8,25,50}

VC-NMD and Gamma-NMD predict lifetimes that are generally larger than the IR limit for LJ argon and its alloys (see Fig. 4). VC-ALD predicts essentially monotonically decreasing lifetimes with increasing frequency for the LJ argon alloys [Fig. 5(a)]. Because VC-NMD and VC-ALD use the same values for $v_g(\nu)$, the phonon mode diffusivities will be underpredicted for VC-ALD compared to VC-NMD for the LJ argon alloys with a significant number of lifetimes below the IR limit (see Fig.). There are thus two underpredictions to consider when interpreting the thermal conductivity predictions in Section : (i) underprediction of the thermal diffusivity that results from using the VC group velocities for VC-NMD and VC-ALD, and (ii) the underprediction of the mode lifetimes for LJ argon alloys by the VC-ALD perturbative models.

IV. THERMAL CONDUCTIVITY PREDICTIONS

The thermal conductivities of the LJ systems can now be predicted from Eq. (1) using the vibrational mode properties predicted by the VC-NMD and VC-ALD methods. Given the discussion regarding the VC-predicted mode properties in Section III E, we also predict ther-

mal conductivity using the equilibrium MD-based GK method, which is a top-down method that does not make any approximations about the nature of the normal modes. Thermal conductivities predicted by the GK method naturally capture all scattering mechanisms.^{32,66,67} The main challenge in the GK method is how to specify the converged value of the thermal conductivity from the integral of the heat current autocorrelation function, which is determined by the maximum of this integral. The heat current was computed every 10 time steps from the same atomic trajectories (positions and velocities) used for the VC-NMD and Gamma-NMD methods.

To predict a bulk thermal conductivity, finite-size extrapolation is used,

$$\frac{k(N_0)}{k_0} = 1 - \frac{c_0}{N_0}, \quad (19)$$

where c_k is a constant, k_0 is the extrapolated bulk thermal conductivity, and $k(N_0)$ is the size-dependent thermal conductivity.¹³ For VC-NMD and VC-ALD, the validity of the finite-size scaling requires that the low frequency modes in the system be dominated by phonon-phonon scattering (i.e. $\tau \propto \omega^{-2}$) and follow the Debye approximation with respect to the group velocity DOS.^{13,14} For LJ argon alloys, this requirement is satisfied for modest system sizes (for $N_0 = 6$ to 12) so that both VC-NMD and VC-ALD predictions can be extrapolated to a bulk value. For SW silicon alloys, the thermal conductivity is dominated by low-frequency modes, so that large system sizes are needed to satisfy the extrapolation requirements and only GK and VC-ALD can be used ($N_0 \leq 42$ in the present study, similar to the converged system sizes in⁴¹). This highlights the efficiency of the VC-ALD method, which is necessary when computationally expensive DFT calculations are used (Section).^{4,10,11,14,68,69}

Bulk thermal conductivity predictions are made for VC-NMD, VC-ALD, and GK are tabulated in Table I and plotted in Fig. 7. While agreement between the three methods is found for the perfect crystal, VC-NMD and VC-ALD underpredict the alloy thermal conductivities compared to GK. Also plotted is the high-scatter thermal conductivity prediction k_{HS} (Eq. (3)). The underprediction is modest for VC-NMD, 20% or less for all concentrations. In Section III D, we argued for the existence of a minimum mode thermal diffusivity, D_{HS} . As shown in Fig. , the diffusivities of many high-frequency modes in the LJ alloys, predicted by both VC-NMD and VC-ALD, fall below this limit. Based on this observation, we propose that any thermal diffusivity below the limit be set to D_{HS} . The results of this adjustment, referred to as VC-NMD* and VC-ALD*, are plotted in Fig. 7. The adjusted

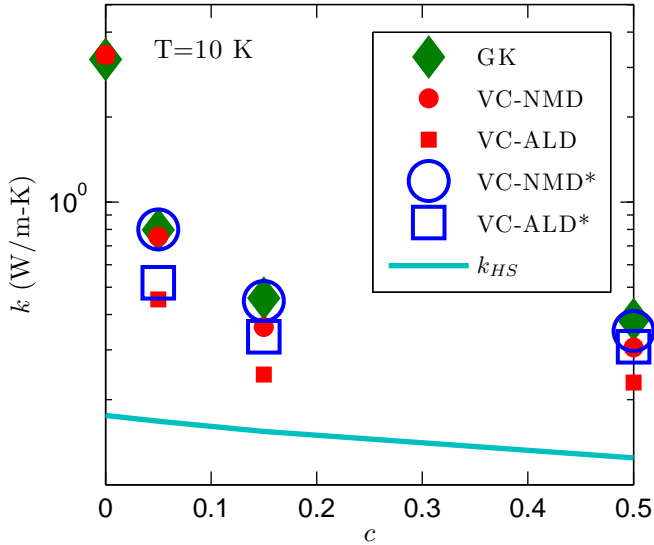


FIG. 7: Thermal conductivity predictions for LJ argon alloys at $T=10$ K using the VC-NMD, VC-ALD, and GK methods. The high-scatter thermal conductivity prediction k_{HS} (see Eq. (3)) and the high-scatter adjusted VC-NMD* and VC-ALD* are also plotted. The adjusted VC-NMD* is brought into agreement with GK method predictions, while the correction VC-ALD* is only marginally changed.

thermal conductivities predicted by VC-NMD* are within 10% of GK for all concentrations. Combined with D_{HS} , the VC-NMD predicted thermal diffusivities are good representations for the explicitly disordered modes present in the MD simulation.

The VC-ALD method underpredicts the thermal conductivity of the LJ argon alloys, where the underprediction is worst for a concentration of 0.05, k_{VC-ALD}/k_{GK} is 0.56. By applying the high-scatter limit adjustment VC-ALD*, the thermal conductivities are brought into marginally better agreement, worst for a concentration of 0.05, where k_{VC-ALD^*}/k_{GK} is 0.65. The VC-ALD method fails to accurately predict the high-frequency mode thermal diffusivities for LJ argon alloys, which can be seen in Fig. 5 (b). Since the group velocities are the same for VC-NMD and VC-ALD, the underprediction of the high-frequency thermal diffusivities, and hence thermal conductivity, is due to the underprediction of the high-frequency mode lifetimes [Fig. 5(a)]. Thus the adjustment VC-ALD* fails to bring VC-ALD into agreement with VC-NMD and GK.

TABLE I: Thermal conductivity predictions using the VC-NMD, VC-ALD, and GK method. For LJ argon alloys, the bulk extrapolation is used for all 3 methods. For SW silicon alloys, only VC-ALD and GK can be used to extrapolate a bulk thermal conductivity (see Section IV).

c	VC-NMD	VC-ALD	VC-NMD*	VC-ALD*	GK
LJ					
0.00	3.33 ± 0.12	3.45 ± 0.05			3.27 ± 0.09
0.05	0.76 ± 0.07	0.45 ± 0.05	0.80 ± 0.07	0.52 ± 0.05	0.80 ± 0.07
0.15	0.36 ± 0.04	0.24 ± 0.03	0.45 ± 0.05	0.33 ± 0.07	0.46 ± 0.07
0.50	0.31 ± 0.04	0.23 ± 0.03	0.35 ± 0.05	0.31 ± 0.07	0.38 ± 0.07
SW					
0.00		484 ± 21			517 ± 33
0.05		23.5 ± 1.9		23.7 ± 1.9	20.1 ± 1.5
0.15		11.9 ± 0.9		12.0 ± 0.9	9.90 ± 0.9
0.50		11.1 ± 0.9		11.2 ± 0.9	9.30 ± 0.9

V. SW SILICON

Because of the discrepancies between the VC-NMD and VC-ALD predicted mode properties and thermal conductivities for the LJ argon alloys, we now predict the mode properties and thermal conductivity for SW silicon alloys which are “stiffer” (larger phonon group velocities and lifetimes). The lifetimes for a concentration of 0.5 predicted by VC-NMD and VC-ALD are plotted in Fig. 8(a). The VC-NMD predicted lifetimes are generally larger than the IR limit for SW silicon alloys, similar to VC-NMD predictions for the LJ argon alloys (Fig. 4). Unlike the LJ argon alloys, the VC-NMD and VC-ALD predicted lifetimes agree over most of the frequency spectrum, except at the highest frequencies, where VC-ALD underpredicts VC-NMD and falls below the IR limit. The high-frequency plateau of the VC-NMD predicted mode lifetimes for LJ argon (Fig. 4) is not seen for SW silicon.

As shown in Fig. 8(c), the thermal conductivity of SW silicon alloys is dominated by low-frequency modes. As seen in Figs. 5(b) and 8(b), VC-NMD and VC-ALD both predict a significant number of modes with $D_{ph}(\nu) < D_{HS}$ for both the LJ argon and SW silicon alloys.

For SW silicon, we can only make bulk thermal conductivity predictions for VC-ALD and GK (see Table I and Fig. 9) because computational demands limit the system sizes accessible with VC-NMD. From Table I, the thermal conductivities predicted for SW silicon alloys by VC-ALD and GK are in agreement within less than 20%, even without the adjustment VC-ALD*, where VC-ALD actually overpredicts compared to GK. The predicted thermal conductivities for SW silicon alloys at all concentrations is over an order of magnitude larger than the high-scatter prediction k_{HS} (Eq. (3)). Because thermal transport in SW silicon is low-frequency dominant, however, the high-scatter adjustments VC-NMD* and VC-ALD* vary by only one percent compared to the unadjusted VC-NMD and VC-ALD.

For the large concentrations and mass ratios considered in this work, the terms higher order terms in the Tamura perturbation theory are order 1 and larger at high frequencies (see Section).¹ It is possible that higher-order interactions in the Tamura theory are also responsible for the discrepancy of the lifetimes predicted by VC-NMD and VC-ALD in SW silicon at the highest frequencies, but this discrepancy is unimportant to the overall thermal transport.

The LJ argon and SW silicon alloys studied in this work have different ranges of phonon

frequencies, lifetimes, group velocities, and total thermal conductivity. For bulk silicon, the thermal conductivity is dominated by low-frequency modes,^{5,11,30,31} which is also true for bulk and alloyed SW silicon (see Fig. 8). For SW silicon, VC-ALD predicts thermal conductivities in reasonable agreement with the explicitly disordered GK method (Fig. 9). For LJ argon, VC-ALD underpredicts the high-frequency phonon lifetimes and thermal diffusivities (see Fig. 5), leading to an underprediction of thermal conductivity when compared to VC-NMD and GK (see Section IV).

The results for the SW silicon and LJ argon alloys suggest that thermal modeling of ordered and disordered lattices can be separated into two broad groups: low-frequency dominated and full-spectrum materials. Materials dominated by low-frequency modes tend to have high thermal conductivities, which is due to their large group velocities and long lifetimes.^{30,31,70,71} These low-frequency modes follow closely the scalings predicted by the perturbative VC-ALD models, which are valid at low-frequencies.

LJ argon is a material whose thermal transport has significant contribution from high-frequency modes, even for the bulk (see Fig. 5 (c)). This high-frequency range is where we predict that the perturbative Tamura theory will have non-negligible contributions from higher-order interactions (see Section III C 2). While the higher-order interactions in the Tamura theory are also predicted to be non-negligible for SW silicon, this does not affect the thermal conductivity predictions significantly because high frequencies are unimportant to thermal transport. This is also true for the thermal conductivity spectrum of SiGe alloys from predictions^{9,11,70} Experimental measurements^{30,31,71} For example, the thermal conductivity of SiGe alloys exceeds the high-scatter limit by more than an order of magnitude at room temperature for all compositions.^{26,30,31}

Based on the thermal conductivity predictions for VC-NMD* and the well-defined peaks in the structure factors (Fig. 3), the reduction of group velocities in disordered lattices due to zone folding seems to be an underprediction of the group velocity of moderate to high frequency modes.⁴⁵

VI. SUMMARY

The concept of simple alloying remains at the forefront of efforts to control or minimize the thermal conductivity of semiconducting and thermoelectric materials (cite SiGe nanoporous,

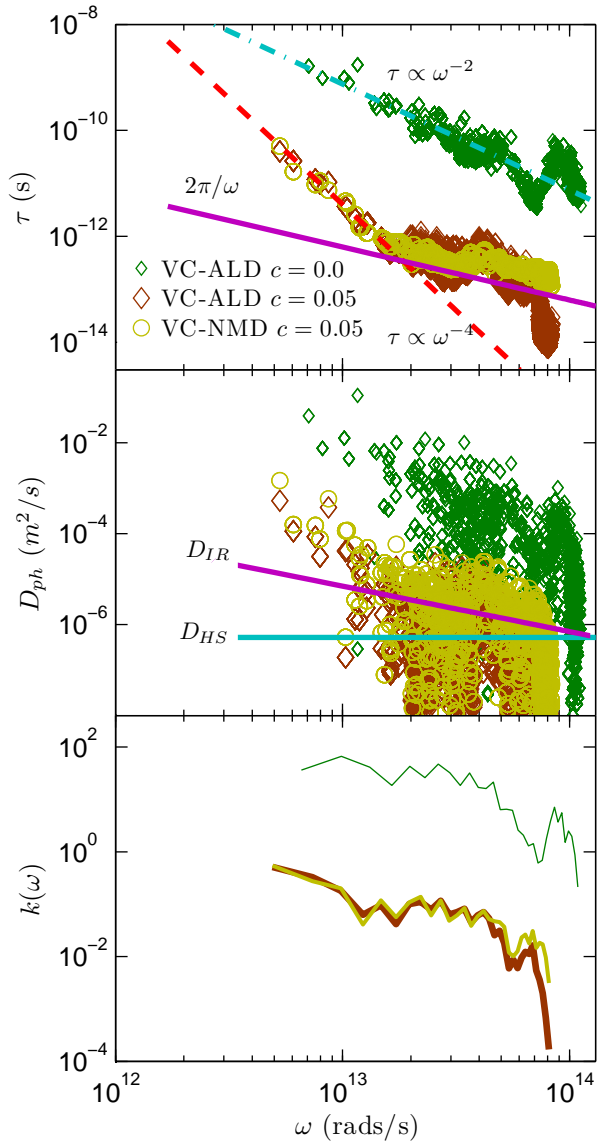


FIG. 8: (a) predicted lifetimes for VC modes using VC-NMD and VC-AID for SW silicon. (b) predicted VC mode thermal diffusivities, compared to the AF,HS limit. (c) the thermal conductivity frequency spectrum, which is peaked at low frequency, in contrast to LJ argon (Fig. 5).

PbTe) Results in this work suggest that the lower limit for the vibrational mode thermal diffusivity in alloys is $(1/3)v_s a$.

The results in this work support the idea of a minimum thermal diffusivity for the vibrations in disordered lattices.(cite) Although this minimum thermal diffusivity is usually interpreted as a minimum mean free path, we find that concept is not necessary for inter-

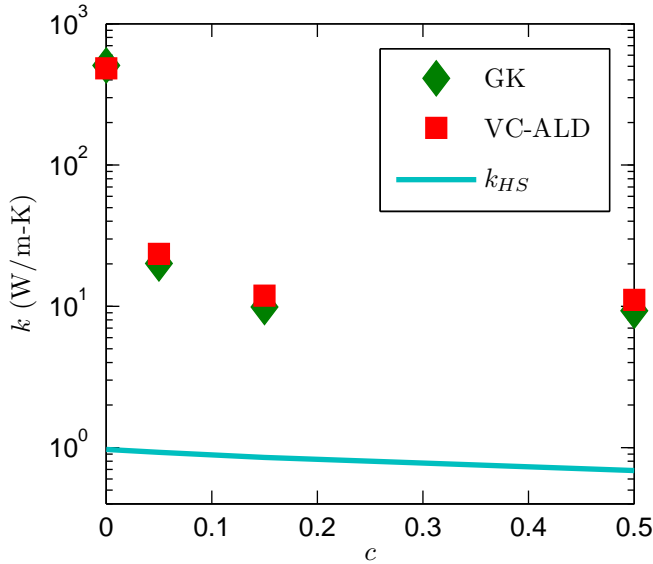


FIG. 9: Thermal conductivity predictions for SW silicon alloys at a temperature of 300 K using the VC-NMD, VC-ALD, and GK methods. The high-scatter thermal conductivity prediction k_{HS} (see Eq. (3)) is also plotted. The adjusted VC-ALD* is not shown since it differs by only one percent compared to VC-ALD. The bulk thermal conductivity cannot be predicted using the VC-NMD method because computational demands limit the system sizes.

preting the results of this work. The VC approximation provides a computationally cheap framework, which is essential for expensive but experimentally accurate *ab initio* methods for predicting thermal conductivity.(cite) The high-scatter limit of thermal diffusivity is more useful for examining the thermal transport in alloys under the framework of the VC approximation. The fundamental quantity is the mode lifetimes and the group velocity is an approximation, and expressed together as thermal diffusivity they can be interpreted in the presence of disorder.

The VC approximation results in two underpredictions for modes at high frequencies: (i) underprediction of the disordered vibrational thermal diffusivities because of the VC predicted group velocities, and (ii) underprediction of the disordered mode lifetimes by the perturbative VC-ALD method. The validity of the VC approximation has been verified for SW silicon alloys, which is a model system dominated by low-frequency modes. The underprediction of both the mode group velocities by the VC and the lifetimes by VC-ALD

occurs at the highest frequencies for SW silicon alloys, but these modes are unimportant to thermal transport. This is the plausible explanation for the success of the VC approximation phenomenologically and predictively for low-frequency dominated, high thermal conductivity materials.(cite)

For LJ argon alloys, which have significant thermal transport from high-frequency modes, VC-NMD and VC-ALD both underpredcit the thermal conductivity compared to the system-level GK method. VC-NMD underpredicts only modestly, and can be brough into good agreement with GK by applying the high-scatter limit adjustment VD-NMD*. For VC-ALD, the high-scatter limit adjustment VC-ALD* still underpredicts compared to GK and VC-NMD*, suggesting that the perturbative Tamura theory is not appropriate for LJ argon alloys. This may be true for the high-frequency modes of any disordered lattice,(cite) and the high-scatter limit $D_{AF,HS}$ should be considered whenever the perturbative VC-ALD method is used.

Acknowledgments

This work is supported by AFOSR award FA95501010098. This work was supported in part by a grant of computer time from the DOD High Performance Computing Modernization Program at the US Army Engineer Research and Development Center. We thank Joseph Feldman, Jivtesh Garg, Zhiteng Tian, Davide Donadio, Asad Hasan and Craig Maloney for helpful discussions.

Appendix A: NMD using Non-Exact Normal Modes

For a normal mode of the lattice supercell used for the MD simulations, the autocorrelation of the total normal mode enery autocorrelations are damped exponentials with a decay time $\tau(\kappa_\nu)$ and the kinetic energy autocorrelation is a cosinusodial exponentially-damped oscillation with frequency $2\omega(\kappa_\nu)$.(cite AHRT) When using the VC normal modes to map the MD simulation trajectories from the explicitly disordered lattice supercells, the mode total and kinetic energy autocorrelation fucntions do not always follow the simple functional forms, see Fig. 10 (a) and (b). By calculating the phonon mode spectral energy Φ , which is a phonon mode energy method in the frequency-domain,²⁴ artifacts such as multiple peaks

in a given mode's energy spectrum Φ can be observed for high concentrations, $c = 0.5$, Fig. 10 (a).

These artifacts in the mode energy spectrum and autocorrelations are not surprising given two considerations: (i) the MD simulations contain explicit disorder which influences the atomic trajectories, (ii) the VC normal modes are not the exact normal modes and of the explicitly disordered lattice supercells. It is important to remember that the VC normal modes are exact in the limit $c - > 0$.

In the case of multiple peaks in the VC phonon mode spectrum Φ , the choice of which peak to fit to predict the phonon properties can be ambiguous. An effective lifetime can be predicted unambiguously using Eq. (11) because the VC phonon mode autocorrelations still decay to zero in a finite time, Fig. 10 (b). This results is to be expected given that the atomic trajectories contain information about the lattice energy, which from general statistical physics principles will have exponential relaxation behavior in an equilibrium ensemble.⁷²⁻⁷⁴

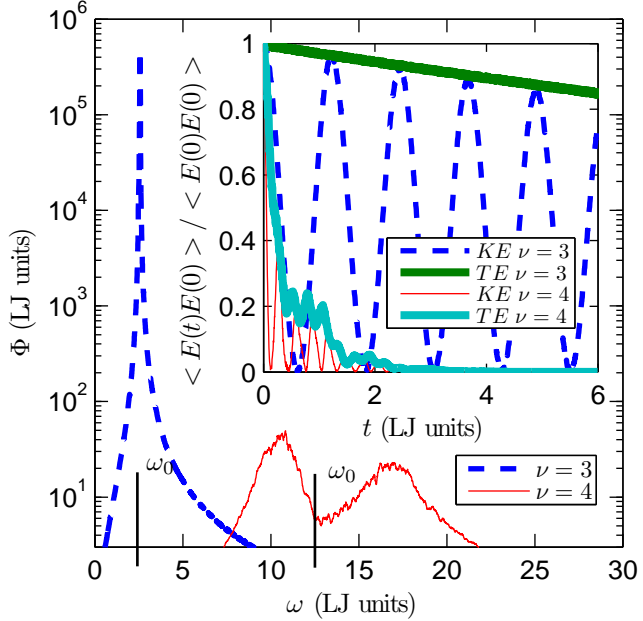


FIG. 10: The spectral energy density Φ of two modes (polarizations $\nu = 3, 4$ at wavevector $[0.2 \ 0]$) calculated using VC-NMD for a mass disordered LJ FCC supercell ($N_0 = 8$ and $c = 0.5$). The VC dispersion-predicted peaks are labeled by ω_0 . Inset: the same mode's energy (kinetic (KE) and total (TE)) autocorrelation functions. Note the additional harmonic effects in the KE and TE autocorelation functions for $\nu = 4$ which are due to the double peaks in Φ . A mode lifetime can be extracted unambiguously using the integral of the TE autocorrelation function (Section III C 1).

-
- * Electronic address: mcgaughhey@cmu.edu
- ¹ S.-i. Tamura, Phys. Rev. B **27**, 858866 (1983), URL <http://link.aps.org/doi/10.1103/PhysRevB.27.858>.
- ² Y. K. Koh, C. J. Vineis, S. D. Calawa, M. P. Walsh, and D. G. Cahill, Applied Physics Letters **94**, 153101 (2009), URL <http://link.aip.org/link/?APL/94/153101/1>.
- ³ B. Qiu, H. Bao, G. Zhang, Y. Wu, and X. Ruan, Computational Materials Science **53**, 278 (2012), ISSN 0927-0256, URL <http://www.sciencedirect.com/science/article/pii/S0927025611004770>.
- ⁴ Z. Tian, J. Garg, K. Esfarjani, T. Shiga, J. Shiomi, and G. Chen, Phys. Rev. B **85**, 184303 (2012), URL <http://link.aps.org/doi/10.1103/PhysRevB.85.184303>.
- ⁵ B. Abeles, Phys. Rev. **131**, 19061911 (1963), URL <http://link.aps.org/doi/10.1103/PhysRev.131.1906>.
- ⁶ J. M. Ziman, *Electrons and Phonons* (Oxford, New York, 2001).
- ⁷ J. L. Feldman, M. D. Kluge, P. B. Allen, and F. Wooten, Physical Review B **48**, 1258912602 (1993).
- ⁸ P. B. Allen, J. L. Feldman, J. Fabian, and F. Wooten, Philosophical Magazine B **79**, 1715 (1999).
- ⁹ A. Ward and D. A. Broido, Phys. Rev. B **81**, 085205 (2010), URL <http://link.aps.org/doi/10.1103/PhysRevB.81.085205>.
- ¹⁰ L. Lindsay, D. A. Broido, and T. L. Reinecke, Phys. Rev. Lett. **109**, 095901 (2012), URL <http://link.aps.org/doi/10.1103/PhysRevLett.109.095901>.
- ¹¹ J. Garg, N. Bonini, B. Kozinsky, and N. Marzari, Phys. Rev. Lett. **106**, 045901 (2011), URL <http://link.aps.org/doi/10.1103/PhysRevLett.106.045901>.
- ¹² T. Shiga, J. Shiomi, J. Ma, O. Delaire, T. Radzynski, A. Lusakowski, K. Esfarjani, and G. Chen, Phys. Rev. B **85**, 155203 (2012), URL <http://link.aps.org/doi/10.1103/PhysRevB.85.155203>.
- ¹³ J. Shiomi, K. Esfarjani, and G. Chen, Physical Review B **84**, 104302 (2011).
- ¹⁴ K. Esfarjani, G. Chen, and H. T. Stokes, Physical Review B **84**, 085204 (2011).
- ¹⁵ N. d. Koker, Physical Review Letters **103**, 125902 (2009), URL <http://link.aps.org/>

- abstract/PRL/v103/e125902.
- ¹⁶ H. Bao, B. Qiu, Y. Zhang, and X. Ruan, Journal of Quantitative Spectroscopy and Radiative Transfer **113**, 1683 (2012), ISSN 0022-4073, URL <http://www.sciencedirect.com/science/article/pii/S0022407312002336>.
- ¹⁷ N. W. Ashcroft and N. D. Mermin, *Solid State Physics* (Saunders, Fort Worth, 1976).
- ¹⁸ F. H. Stillinger and T. A. Weber, Physical Review B **31**, 52625271 (1985).
- ¹⁹ G. C. Sosso, D. Donadio, S. Caravati, J. Behler, and M. Bernasconi, Phys. Rev. B **86**, 104301 (2012), URL <http://link.aps.org/doi/10.1103/PhysRevB.86.104301>.
- ²⁰ R. Peierls, *Quantum Theory of Solids* (Oxford University Press, 2001).
- ²¹ D. A. Broido, M. Maloney, G. Birner, N. Mingo, and D. Stewart, Applied Physics Letters **91**, 231922 (2007).
- ²² A. Ward, D. A. Broido, D. A. Stewart, and G. Deinzer, Phys. Rev. B **80**, 125203 (2009).
- ²³ D. A. McQuarrie, *Statistical Mechanics* (University Science Books, Sausalito, 2000).
- ²⁴ J. M. Larkin, J. E. Turney, A. D. Massicotte, C. H. Amon, and A. J. H. McGaughey, submitted to Journal of Computational and Theoretical Nanoscience. yes, yes (2012).
- ²⁵ P. B. Allen and J. L. Feldman, Physical Review B **48**, 1258112588 (1993).
- ²⁶ D. Cahill and R. Pohl, Annual Review of Physical Chemistry **39**, 93121 (1988).
- ²⁷ P. G. Klemens, Proceedings of the Physical Society. Section A **68** (1955).
- ²⁸ P. G. Klemens, Proceedings of the Physical Society. Section A **70**, 833 (1957), URL <http://stacks.iop.org/0370-1298/70/i=11/a=407>.
- ²⁹ J. Callaway, Physical Review **113**, 1046 (1959).
- ³⁰ D. G. Cahill and F. Watanabe, Phys. Rev. B **70**, 235322 (2004), URL <http://link.aps.org/doi/10.1103/PhysRevB.70.235322>.
- ³¹ D. G. Cahill, F. Watanabe, A. Rockett, and C. B. Vining, Phys. Rev. B **71**, 235202 (2005), URL <http://link.aps.org/doi/10.1103/PhysRevB.71.235202>.
- ³² A. Skye and P. K. Schelling, Journal of Applied Physics **103**, 113524 (2008), URL <http://link.aip.org/link/?JAP/103/113524/1>.
- ³³ D. C. Mattis, Phys. Rev. **107**, 17361736 (1957), URL <http://link.aps.org/doi/10.1103/PhysRev.107.1736.3>.
- ³⁴ W. A. Kamitakahara and B. N. Brockhouse, Phys. Rev. B **10**, 12001212 (1974), URL <http://link.aps.org/doi/10.1103/PhysRevB.10.1200>.

- ³⁵ I. Kudman, Journal of Materials Science **7**, 1027 (1972), ISSN 0022-2461, URL <http://dx.doi.org/10.1007/BF00550066>.
- ³⁶ Y. Pei, X. Shi, A. LaLonde, H. Wang, L. Chen, and G. J. Snyder, Nature **473**, 66 (2011), ISSN 0028-0836, URL <http://dx.doi.org/10.1038/nature09996>.
- ³⁷ K. Momma and F. Izumi, Journal of Applied Crystallography **41**, 653658 (2008), URL <http://dx.doi.org/10.1107/S0021889808012016>.
- ³⁸ S. Plimpton, Journal of Computational Physics **117**, 1 (1995), ISSN 0021-9991, URL <http://www.sciencedirect.com/science/article/pii/S002199918571039X>.
- ³⁹ J. D. Gale and A. L. Rohl, Molecular Simulation **29**, 291 (2003).
- ⁴⁰ J. V. Goicochea, M. Madrid, and C. H. Amon, Journal of Heat Transfer **132**, 012401 (2010).
- ⁴¹ Y. He, I. Savic, D. Donadio, and G. Galli, Phys. Chem. Chem. Phys. pp. – (2012), URL <http://dx.doi.org/10.1039/C2CP42394D>.
- ⁴² D. P. Sellan, J. E. Turney, A. J. H. McGaughey, and C. H. Amon, Journal of Applied Physics **108**, 113524 (2010).
- ⁴³ A. J. H. McGaughey, PhD thesis, University of Michigan, Ann Arbor, MI (2004).
- ⁴⁴ A. M. Bouchard, R. Biswas, W. A. Kamitakahara, G. S. Grest, and C. M. Soukoulis, Phys. Rev. B **38**, 1049910506 (1988), URL <http://link.aps.org/doi/10.1103/PhysRevB.38.10499>.
- ⁴⁵ J. C. Duda, T. S. English, D. A. Jordan, P. M. Norris, and W. A. Soffa, Journal of Physics: Condensed Matter **23**, 205401 (2011), URL <http://stacks.iop.org/0953-8984/23/i=20/a=205401>.
- ⁴⁶ A. J. H. McGaughey and M. Kaviany, in *Advances in Heat Transfer, Volume 39*, edited by G. A. Greene, Y. I. Cho, J. P. Hartnett, and A. Bar-Cohen (Elsevier, 2006), p. 169255.
- ⁴⁷ Y. He, D. Donadio, J.-H. Lee, J. C. Grossman, and G. Galli, ACS Nano **5**, 1839\961844 (2011).
- ⁴⁸ Y. He, D. Donadio, and G. Galli, Applied Physics Letters **98**, 144101 (2011).
- ⁴⁹ D. Donadio and G. Galli, Phys. Rev. Lett. **102**, 195901 (2009).
- ⁵⁰ J. L. Feldman, P. B. Allen, and S. R. Bickham, Phys. Rev. B **59**, 35513559 (1999), URL <http://link.aps.org/doi/10.1103/PhysRevB.59.3551>.
- ⁵¹ S. Volz and G. Chen, Physical Review B **61**, 26512656 (2000).
- ⁵² N. L. Green, D. Kaya, C. E. Maloney, and M. F. Islam, Physical Review E **83**, 051404 (2011), URL <http://link.aps.org/doi/10.1103/PhysRevE.83.051404>.
- ⁵³ A. J. C. Ladd, B. Moran, and W. G. Hoover, Physical Review B **34**, 50585064 (1986).

- ⁵⁴ J. E. Turney, PhD thesis, Carnegie Mellon University, Pittsburgh, PA (2009).
- ⁵⁵ M. T. Dove, *Introduction to Lattice Dynamics* (Cambridge, Cambridge, 1993).
- ⁵⁶ S. N. Taraskin and S. R. Elliott, Philosophical Magazine Part B **79**, 17471754 (1999), URL <http://www.tandfonline.com/doi/abs/10.1080/13642819908223057>.
- ⁵⁷ D. J. Ecsedy and P. G. Klemens, Phys. Rev. B **15**, 59575962 (1977), URL <http://link.aps.org/doi/10.1103/PhysRevB.15.5957>.
- ⁵⁸ A. A. Maradudin and A. E. Fein, Physical Review **128**, 25892608 (1962).
- ⁵⁹ N. Xu, V. Vitelli, M. Wyart, A. J. Liu, and S. R. Nagel, Phys. Rev. Lett. **102**, 038001 (2009), URL <http://link.aps.org/doi/10.1103/PhysRevLett.102.038001>.
- ⁶⁰ S. Shenogin, A. Bodapati, P. Keblinski, and A. J. H. McGaughey, Journal of Applied Physics **105**, 034906 (2009), URL <http://link.aip.org/link/?JAP/105/034906/1>.
- ⁶¹ P. Sheng, *Introduction to Wave Scattering: Localization and Mesoscopic Phenomena* (Springer, 2006), ISBN 9783540291565.
- ⁶² V. Vitelli, N. Xu, M. Wyart, A. J. Liu, and S. R. Nagel, Phys. Rev. E **81**, 021301 (2010), URL <http://link.aps.org/doi/10.1103/PhysRevE.81.021301>.
- ⁶³ P. Sheng and M. Zhou, Science **253**, 539542 (1991), URL <http://www.sciencemag.org/content/253/5019/539.abstract>.
- ⁶⁴ C. Kittel, Physical Review **75**, 974 (1949).
- ⁶⁵ J. E. Graebner, B. Golding, and L. C. Allen, Phys. Rev. B **34**, 56965701 (1986), URL <http://link.aps.org/doi/10.1103/PhysRevB.34.5696>.
- ⁶⁶ E. S. Landry, M. I. Hussein, and A. J. H. McGaughey, Physical Review B **77**, 184302 (2008).
- ⁶⁷ E. S. Landry and A. J. H. McGaughey, Physical Review B **79**, 075316 (2009).
- ⁶⁸ K. Esfarjani and H. T. Stokes, Physical Review B **77**, 144112 (2008).
- ⁶⁹ L. Chaput, A. Togo, I. Tanaka, and G. Hug, Phys. Rev. B **84**, 094302 (2011), URL <http://link.aps.org/doi/10.1103/PhysRevB.84.094302>.
- ⁷⁰ B. Abeles, D. S. Beers, G. D. Cody, and J. P. Dismukes, Phys. Rev. **125**, 4446 (1962), URL <http://link.aps.org/doi/10.1103/PhysRev.125.44>.
- ⁷¹ R. Cheaito, J. C. Duda, T. E. Beechem, K. Hattar, J. F. Ihlefeld, D. L. Medlin, M. A. Rodriguez, M. J. Campion, E. S. Piekos, and P. E. Hopkins, Phys. Rev. Lett. **109**, 195901 (2012), URL <http://link.aps.org/doi/10.1103/PhysRevLett.109.195901>.
- ⁷² G. P. Srivastava, *The Physics of Phonons* (Adam Hilger, Bristol, 1990).

- ⁷³ L. Landau, E. Lifshitz, and L. Pitaevskii, *Statistical Physics, Part 2 : Volume 9, Pt 2* (Elsevier Science & Technology Books, 1980), ISBN 9780750626361, URL <http://books.google.com/books?id=NaB7oAk09MC>.
- ⁷⁴ A. Rajabpour and S. Volz, Journal of Applied Physics **108**, 094324 (2010), URL <http://link.aip.org/link/?JAP/108/094324/1>.
- **
- ⁷⁵ For a finite-size system, the delta function in Eq. (5) is broadened using a Lorentzian function with a full-width at half maximum set to $20\delta_{\omega,\text{avg}}$, where $\delta_{\omega,\text{avg}}$ is the average frequency spacing.⁵⁰ ††
- ⁷⁶ To perform the calculation of Eq. (14), it is necessary to broaden the discrete frequencies using a Lorentzian function.¹ For all calculations, the Lorentzian was broadened using a value of $100\delta_{\omega,\text{avg}}$. For the system sizes here, the results do not differ significantly if this broadening value is varied manually or by increasing system size N_0 . ‡‡
- ⁷⁷ The Cahill-Pohl (CP) and AF HS limit differ by approximately %20.²⁶ ¶¶
- ⁷⁸ For a finite system, the AF theory requires a broadening in frequency to predict the mode-specific thermal diffusivities.²⁵ We use a Lorentzian broadening with a width of $\delta_{\omega,\text{avg}}$. §§
- ⁷⁹ For the disordered lattices studied in this work for $c \leq 0.15$, the predicted k_{AF} is strongly system size dependent, indicating this diverging behavior. For LJ argon alloys at $c = 0.5$, the divergence with system size is small for the range of system size studied ($N_0 = 4$ to $N_0 = 12$), where $k_{AF}/k_{GK} = 0.93$ for $N_0 = 12$ because the finite system size limits the thermal diffusivities of the lowest frequencies. ****
- ⁸⁰ The overprediction of thermal conductivity by VC-ALD may be related to the role of disorder in the ALD calculation.^{11,54} While Garg et al found an overprediction of VC-ALD compared to experiment by a factor of two, the overprediction we observe in this work for SW silicon alloys is not as drastic.